Materials Advances

ROYAL SOCIETY OF CHEMISTRY

COMMUNICATION

View Article Online
View Journal | View Issue

Cite this: *Mater. Adv.*, 2021, 2, 4610

Received 31st March 2021,
Accepted 10th June 2021

DOI: 10.1039/d1ma00288k

rsc.li/materials-advances

Metal cation s lone-pairs increase octahedral tilting instabilities in halide perovskites†

Lingyuan Gao, ‡*[a] Lena Yadgarov, ‡*[b] Rituraj Sharma,[b] Roman Korobko,[b] Kyle M. McCall,[c] Douglas H. Fabini,[d] Constantinos C. Stoumpos,[e] Mercouri G. Kanatzidis,[c] Andrew M. Rappe[a] and Omer Yaffe[b]

Halide perovskites exhibit beneficial opto-electronic properties (*e.g.* long carrier lifetimes and low defect densities), and their dynamic structural instabilities and anharmonic thermal fluctuations are directly implicated in these properties. In this work, we combine in-depth analysis of Raman spectroscopy and *ab initio* calculations to uncover the critical roles of Group 14 M^{2+} (M = Pb, Sn, Ge) metal cation s orbital lone pairs in the dynamic instabilities of $CsMBr_3$ and particularly in governing the octahedral tilting. Previous studies concluded that the lone-pair stereochemical activity primarily leads to the off-centering motion of the metal cation, and the tilting is usually ascribed to ionic size effects. Here, we show that the lone-pair stereochemical activity contributes to strong octahedral tilting instabilities that induce liquid-like behavior in all examined crystals, which underlies the robustness of halide perovskites to charged defects. In addition, the lone-pairs induce a local, molecule-like behavior of the Ge^{2+} with a pyramidal bonding motif in the cubic phase, and they contribute to another phase transition of $CsSnBr_3$ at 60 K. Our findings elucidate the fundamental origin of anharmonicities in halide perovskites and provide the crucial link between chemical composition and opto-electronic properties, opening opportunities for lead-free and solution-processable photovoltaics.

Introduction

Halide perovskites (HPs) are extensively studied as potential replacements for the traditional photovoltaic materials.[1] Lead-based HPs have demonstrated solar power conversion efficiencies surpassing 25% in thin films and 29% in tandem cells with Si.[2] This motivates recent efforts to develop new photovoltaic cells that are based on nontoxic perovskite halides, where Pb^{2+} is replaced with Sn^{2+} and/or Ge^{2+}.[3–7]

From a fundamental standpoint, the fascinating opto-electronic properties of HPs are closely related to their highly anharmonic thermal motions that lead to local, polar fluctuations and thus, localization of charge carriers.[8–11,75] The perovskite crystal (with stoichiometry AMX_3) consists of a three-dimensional network of corner-sharing MX_6 octahedra, with A-site cations occupying the cuboctahedral voids. The high connectivity allows for various lower-symmetry phases, characterized by tilting of the octahedra, making HPs capable of accommodating a wide range of compositions.[12,13] This compositional flexibility enables a plethora of phenomena, tuned by competing short- and long–range anharmonic couplings, leading to polar, magnetic, and tilting phase transitions.[14–18]

Geometric or ionic (hard sphere packing) models, which are based only on the sizes of the constituent ions ($r_{A,M,X}$), hold great predictive power for whether a perovskite will form.[19–23] The tolerance factor, $t = \frac{r_A + r_X}{\sqrt{2}(r_M + r_X)}$ of Goldschmidt[19] is the most successful geometric parameter for perovskite prediction: if $t > 1$, then the A-site cation is too large to fit in the MX_6 cuboctahedral cavities, and that disfavors the formation of a perovskite. If $t < 1$, then the A-site cation is relatively small for the interstitial region between octahedra, and so the corner-sharing octahedra tilt to fill the space. Following different tilting patterns, many low-symmetry structures can be formed due to this tilting instability.[21–31] The tilting can also be dynamic, resulting in structural fluctuations.[8,9,14,32–36] When t is too low, the corner-sharing

[a] *Department of Chemistry, University of Pennsylvania, Philadelphia, Pennsylvania 19104-6323, USA. E-mail: rappe@sas.upenn.edu*
[b] *Department of Chemical and Biological Physics, Weizmann Institute of Science, Rehovot 76100, Israel. E-mail: omer.yaffe@weizmann.ac.il*
[c] *Department of Chemistry, Northwestern University, Evanston, Illinois 60208, USA*
[d] *Max Planck Institute for Solid State Research, Stuttgart 70569, Germany*
[e] *Department of Materials Science and Technology, University of Crete, Voutes Campus, Heraklion 70013, Greece*

† Electronic supplementary information (ESI) available. See DOI: 10.1039/d1ma00288k

‡ These authors contributed equally.

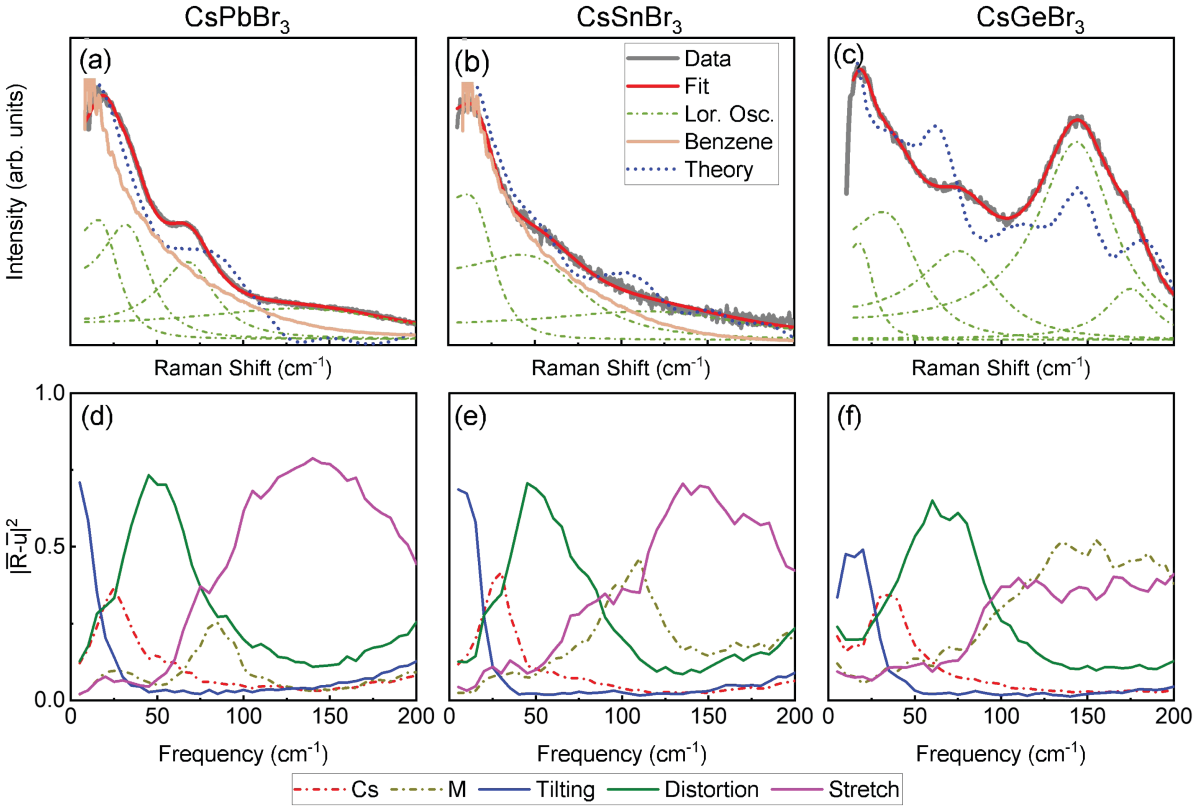

Fig. 1 Upper Panel: high temperature, cubic phase Raman spectra of $CsPbBr_3$, $CsSnBr_3$, and $CsGeBr_3$ single crystals. Lower Panel: projections of frequency-filtered MD for the three crystals. The dominance of the central peak decreases as the ionic size decreases, indicating that the relaxational tilting has an opposite trend compared with stereochemical activities.

octahedra prefer to rearrange into edge-sharing or face-sharing octahedra,[37] taking the system away from the perovskite structure. In addition to t, the octahedral factor $\mu = r_M/r_X$ is another important geometric factor. According to Pauling's first rule,[20] μ should be large enough to guarantee that the M cation makes contact with all surrounding X anions. Recent studies construct structural maps *vs.* t and μ and correctly categorize oxides and halides as perovskites or non-perovskites at room temperature.[38–42]

Notably, these geometric models represent an ionic limit and contain no information about covalent bonding. Therefore, they sometimes fail to predict the correct structural phase evolution of compounds with certain electron configurations and bonding preferences.[43,44] Heavier halogen ions have lower electronegativity and stronger covalency, reducing the accuracy and applicability of the hard-sphere ionic models.[38–41] Furthermore, main-group cations in lower oxidation states (*e.g.* Pb^{2+}, Sn^{2+}, Ge^{2+}) retain their outermost s electrons as a nonbonded lone pair.[45–48] This lone pair occupies space, behaves like an additional ligand, and is said to be stereochemically active. Acentric distortions of the coordination environments induced by such lone-pair cations allow an energetically favorable mixing with the ligand (anion) orbitals which is symmetry-forbidden in the undistorted state.[49–53] In oxides such as $PbTiO_3$, $Pb(Zr_{1-x}Ti_x)O_3$, lone-pair cations reside on the A site. The large polar displacements of A cations caused by lone-pair effects give rise to the large polarization and giant piezoelectric responses.[54–58] In HPs, they occupy the M site, and significant M off-centering motions are observed experimentally and computationally.[9,46,59–66] Importantly, previous studies show in HPs off-centering instabilities induced by lone-pairs and tilting instabilities can coexist and are competing with each other.[67,68] The tendency for lone-pair-driven distortion is stronger for lighter cations.[50] In $PbTiO_3$-based solid solutions, the overall effects of both instabilities have been used to predict the morphotropic phase boundary (MPB) composition and the transition temperature at the MPB.[69]

Here, we aim to study the interplay between geometric (ionic size) and lone-pair (covalency) effects on the structural dynamics of halide perovskites. To that end, we combine Raman spectroscopy and *ab initio* molecular dynamics to compare the structural dynamics of $CsMBr_3$ in their cubic (with M = Pb, Sn, and Ge) and orthorhombic (M = Pb, Sn) phases. This chemical series tunes both the energy scale of the lone-pair-driven distortions and the relative ionic sizes which are the basis for the geometric models. Therefore, changing the central M cation provides an excellent means of establishing the relative importance of concurrent size and covalence effects in the structural dynamics of the HPs. In our analysis, we go beyond the harmonic approximation[68,70] as we assign real-space motion from *ab initio* molecular dynamics to the experimentally observed spectral features.

Our main new finding is that the lone pair contributes significantly to octahedral tilting instabilities that go beyond what is predicted by geometric models. These fluctuations give rise to strong, diffuse inelastic light scattering that increases towards 0 cm^{-1} (''central peak'') that is similar to that of liquids. In addition to tilting, the strong lone-pair stereochemical activity also induces dynamic Ge^{2+} off-centering motions as dynamic fluctuations between pyramidal environments in $CsGeBr_3$ that are uncorrelated to neighbors, leading to a molecule-like behavior. At around 60 K, in $CsSnBr_3$ the lone pair contributes to another phase transition to lower symmetry phase. We expect these lone-pair driven structural instabilities discovered in $CsMBr_3$ also prevail in their organic HP counterparts, which are more widely used in photovoltaics.[76]

Results and discussion

We begin our study by comparing the structural dynamics of $CsPbBr_3$, $CsSnBr_3$, and $CsGeBr_3$ in their cubic phases ($Pm\bar{3}m$, space group #221). A detailed discussion of the phase sequence, ionic size and lone-pair stereochemical activity of the three crystals is given in the section ''Inadequacy of ionic size models'' of ESI.† It is important to note that based on the symmetry of average structure, the crystals should be Raman inactive.[71] Yet, as shown in Fig. 1(a)–(c) all three crystals show strong, first order Raman scattering. The failure of factor group analysis to predict the Raman spectra is an important indication that the thermal fluctuations of all three crystals are strongly anharmonic. The dash-and-dot lines show the spectral features that are extracted from a fit of each spectrum to the product of the Bose–Einstein distribution and a sum of damped Lorentz oscillators (see ESI† for fitting procedures).

Next, we performed *ab initio* molecular dynamics (AIMD) at relevant temperatures (500 K, 330 K and 663 K for $CsPbBr_3$, $CsSnBr_3$, and $CsGeBr_3$, respectively) and calculated dynamic Raman spectra based on AIMD trajectories (calculation details are in the Section ''computational methods'' of ESI†). As shown in Fig. 1, theoretical spectra well reproduce experimental Raman spectra of all the compounds.

The spectra of all three crystals consist of a broad feature increasing continuously toward 0 cm^{-1} superimposed by broad shoulders from 50–100 cm^{-1}. The low-frequency broad feature is composed of over-damped Lorentz oscillators (width $\approx$ 50 cm^{-1}). In that sense, their structural dynamics resemble that of a liquid. To demonstrate this point, the spectrum of benzene at room temperature is overlaid in Fig. 1(a) and (b). Contrary to $CsPbBr_3$ and $CsSnBr_3$, the Raman spectrum of $CsGeBr_3$ (Fig. 1(c)) has a dominant spectral feature centered at $\approx$ 148 cm^{-1}.

To elucidate the origin of Raman activity for the three perovskites, we frequency-filter the AIMD trajectories and project them onto normal-mode coordinates that are presented in Fig. 1(d)–(f). The frequency-filtering method and projection method are introduced in the Section ''computational methods'' of ESI.† Below 30 cm^{-1}, for all three crystals, apart from the harmonic Cs motion, Br_6 octahedral tiltings are the most dominant motions, expected for $CsSnBr_3$ and $CsPbBr_3$ due to their low tolerance factor (t = 0.92 and 0.86 respectively) but are surprising for $CsGeBr_3$ that has a near ideal t (see ESI† for more details). Therefore, the tilting instabilities cannot be fully reconciled with a geometric model solely from ionic effects. Nevertheless, consistent with its near-ideal tolerance factor, the projection weight of the octahedral tilting in $CsGeBr_3$ is lower than its counterpart in $CsSnBr_3$ and $CsPbBr_3$. It has been shown in $CsPbF_3$ that the Pb lone pair can determine the tilting pattern and ground-state structure by displacing surrounding anions and modifying the A-site environments.[67] The clear presence of tilting indicates that apart from ionic effects, the lone pair is another source of such instabilities.

Recent density functional theory (DFT) studies predict that in the cubic phase, tilting instabilities can only emerge in $CsSnBr_3$ and $CsPbBr_3$ but not in $CsGeBr_3$.[68,70] This agrees with the geometric analysis but differs from the present results. In DFT, computational analysis of phonons is generally conducted by finding the harmonic vibrations with respect to a reference structure (*e.g.* the highly symmetric cubic aristotype). AIMD samples the realistic, multi-dimensional potential energy surface and visits various thermally-accessible configurations dynamically. On a time scale of several hundred femtoseconds, the dynamic tilting describes the reorientation of the acentrically-distorted octahedra, and induces various and distinct polar fluctuations in different parts of the solid-which leads to the solid exhibiting spectroscopic signatures like those of a liquid (Fig. 1(a)–(c)).[9,10]

In the middle frequency range (50–100 cm^{-1}), motions are dominated by Br_6 distortion, and its peak is at 50 cm^{-1}. The M motion of $CsPbBr_3$ is also in this middle frequency range, while in $CsSnBr_3$ and $CsGeBr_3$ M motions are at higher frequencies, following a trend inverse to the square root of their masses. As shown in Fig. 1(a)–(c), at 70 cm^{-1} there are clear shoulders in $CsPbBr_3$ and $CsGeBr_3$, and a broader shoulder in $CsSnBr_3$. By relating the fitted signatures in Fig. 1(a)–(c) with the peak of motions in Fig. 1(d)–(f), we find that these shoulders result from Br_6 distortion-driven vibrational modes for all three crystals.

We now turn to discussing the origin of the broad and strong spectral feature that is observed only in $CsGeBr_3$ at $\approx$ 148 cm^{-1}. At high frequencies ($>$100 cm^{-1}), the M–Br stretch is similar for all three crystals and is significant in a wide frequency range (magenta lines in Fig. 1(d)–(f)). However, the Raman scattering is very weak in $CsPbBr_3$ and $CsSnBr_3$. Therefore, we ascribe this feature to the Ge off-centering motion. We can expect that Ge will display much stronger off-centering than Pb and Sn for the following reasons related to mass, size, and bonding. First, Br is much closer in mass to Ge^{2+} than to Sn^{2+} and Pb^{2+}, so concerted motions will have more weight on the Ge^{2+} cation. Second, Ge^{2+} is nominally too small for octahedral coordination with Br, so it can rattle within the octahedral void formed by the anions. Lastly, the Ge^{2+} lone pair is strongly stereochemically active, favoring a 3+3 coordination (3 short bonds, 3 long bonds; essentially a $[GeBr_3]^-$

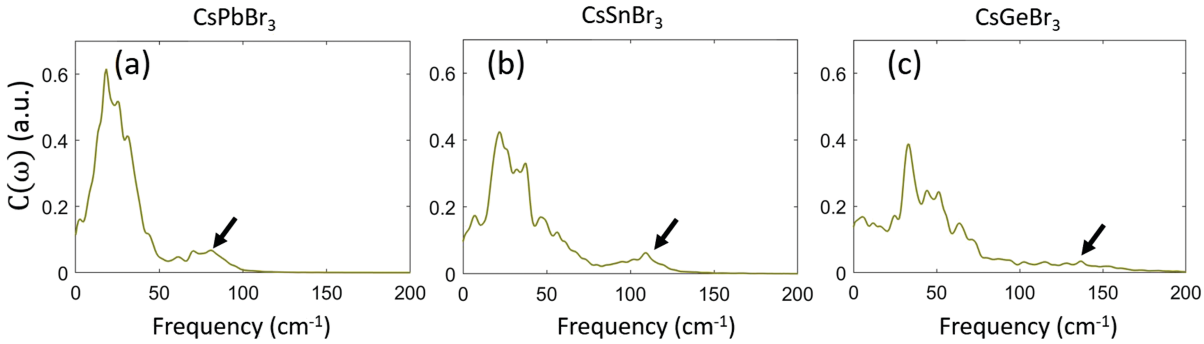

Fig. 2 Computed pair-correlation function of neighbor M atoms in $CsPbBr_3$, $CsSnBr_3$, and $CsGeBr_3$. The arrow denotes M off-centering motions according to their frequencies, identified from Fig. 1. M off-centering motion in $CsGeBr_3$ is less correlated than in $CsPbBr_3$ and $CsSnBr_3$.

pyramid, Fig. S1, ESI†). This relationship with the pyramidal motif is further reinforced by the shape of the $\approx$ 148 cm^{-1} spectral feature in $CsGeBr_3$, which is composed of at least two Lorentz oscillators (Fig. 1(c)). This shape is indicative of the asymmetric stretch ν_3 for a pyramidal molecule with C_{3v} symmetry which is split by the inversion doubling effect.[72,73] As suggested by Thiele *et al.*,[74] the temperature-driven rhombohedral to cubic phase transition is an order–disorder transition, where the cubic long-range ordering is given by the average of these positions but the local structure remains largely pyramidal due to the outsized stereochemical activity of the Ge^{2+} lone pair. The noteworthy high-frequency Raman activity in $CsGeBr_3$ suggests dynamic fluctuations between pyramidal environments that are locally similar to the rhombohedral ground state, with significant Ge^{2+} displacements.

Indeed, from projections of frequency-filtered AIMD, the Ge^{2+} off-centering motions are markedly different from those of Pb^{2+} and Sn^{2+} (yellow trace in Fig. 1(d)–(f)). The latter two show a single-peaked feature within a narrow frequency range, revealing that the M atoms move in a harmonic and collective pattern. As a contrast, $CsGeBr_3$ exhibits a combination of multiple peaks at different frequencies between $\approx$ 140–200 cm^{-1}, indicating the Ge motion is more disordered and local on individual atom and thus the symmetry of the whole crystal has been lowered. To further demonstrate the weakly correlated Ge motion, we compute the pair-correlation function of neighbor M atoms from the AIMD trajectory as:

$$C(\omega) = \mathcal{F}(C(t)) = \int \frac{\left\langle \vec{R}_m(t) \cdot \vec{R}_n(0) \right\rangle}{\left\langle \vec{R}_m(0) \cdot \vec{R}_n(0) \right\rangle} e^{-i\omega t} dt, \qquad (1)$$

where m and n refer to nearest-neighbor M atoms, and $\vec{R}(t)$ is the atomic displacement. Fig. 2 shows that at their corresponding frequencies, off-centering motions between neighboring M atoms in $CsGeBr_3$ are less correlated than in $CsSnBr_3$ and $CsPbBr_3$. This indicates that the motion of the Ge^{2+} ion is more local and behaves like a molecule. Combined with above experimental analysis, we ascribe this high-frequency Raman activity to motion of Ge atom in its low-symmetry local environment.

Summarizing our findings related to the cubic phase of the crystals, we note two different dynamic fluctuations that are related to lone-pair stereochemical activities. The first is the tilting instability that is present in all crystals and results in liquid-like light scattering at low frequencies. The second is the *M*-cation off-centering instability that only leads to molecular-like light scattering in $CsGeBr_3$ at high frequencies. The tilting is stronger in $CsSnBr_3$ and $CsPbBr_3$, with less active lone pairs and smaller tolerance factors, while the off-centering is stronger in $CsGeBr_3$ with more active lone pair and roughly unity tolerance factor. The prominence of these two instabilities is controlled by the interplay of ionic size and covalency effects. Raman signatures of both type of fluctuations are not predicted by models and computations that are based on either the average static structure or the single ground-state structure of these crystals.

We now compare the structural dynamics of the low-temperature orthorhombic phases (*Pnma*, space group #62) of $CsPbBr_3$ and $CsSnBr_3$. This comparison has merit because unlike the cubic phase, this phase has well-defined Raman activity based on its space-group symmetry. $CsGeBr_3$ is excluded from this comparison because, as mentioned previously, it acquires a rhombohedral structure at low temperature. Fig. 3(a) and (b) present the Raman spectra of $CsPbBr_3$ and $CsSnBr_3$ at 80 K, where both crystals are in their orthorhombic phase. The Raman spectrum of $CsPbBr_3$ has only sharp and well resolved Raman peaks that are fitted well by a damped Lorentz oscillator model. Three groups of peaks are identified at 20 cm^{-1}, 50 cm^{-1}, and 80 cm^{-1}, respectively. In contrast, the spectral deconvolution of the $CsSnBr_3$ crystal requires a Debye relaxational component (purple solid line in Fig. 3(b)) in addition to the Lorentz oscillators (see ESI†). This relaxational component indicates that the octahedral instabilities are still significant in $CsSnBr_3$ even at 80 K. Four groups of peaks are identified at 20 cm^{-1}, 40 cm^{-1}, and 60 cm^{-1}, 70 cm^{-1}, respectively. We note that for both compounds, theory and experiments agree very well in terms of the magnitudes and frequencies ($\pm$10 cm^{-1}) of these well resolved Raman-active peaks.

The above statement is supported by our projected AIMD analysis at 80 K (Fig. 3(c) and (d)). First, at low frequency ($<$30 cm^{-1}),

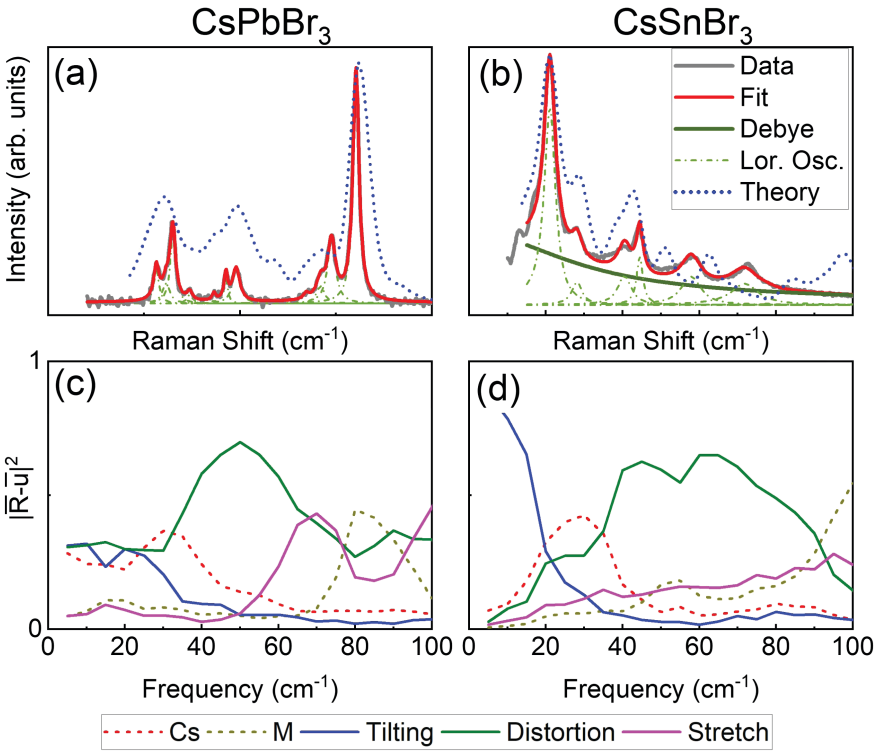

Fig. 3 Upper Panel: low temperature, orthorhombic phase Raman spectra of $CsPbBr_3$, $CsSnBr_3$ single crystals. Lower Panel: projections of frequency-filtered MD for two crystals. The relaxational tilting motion is only present in $CsSnBr_3$ with a larger tolerance factor than that of $CsPbBr_3$. This contradicts with the ionic model which predicts a stronger tilting instability with a smaller tolerance factor.

the tilting motion in $CsSnBr_3$ is dominant (Fig. 3(d)). Its weight continuously decays with increasing frequency, and corresponds to the fitted Debye component in the Raman spectrum (Fig. 3(b)). This is in contrast to what is observed for $CsPbBr_3$ (Fig. 3(c)), where the relaxational behavior of the tilting motion is not as significant as in $CsSnBr_3$, and the low frequency dynamics are also shared by Cs and Br_6 distortion motions. The peak at 30 cm^{-1} in both $CsSnBr_3$ and $CsPbBr_3$ can be ascribed to Cs motion. The peak at 50 cm^{-1} in $CsPbBr_3$ is also assigned to distortion of the octahedra. In $CsSnBr_3$, distortion motions cover a wider frequency range and likely contribute to the Raman peaks at 40 cm^{-1}–80 cm^{-1}. Finally the features between 70 cm^{-1}–90 cm^{-1} in $CsPbBr_3$ are connected with stretching and *M* cation motion.

Similar to the tilting instability of the cubic $CsGeBr_3$ discussed previously, the observed Raman spectra and the results of the projected AIMD analysis for the orthorhombic phases cannot be rationalized by the geometric model that predicts stronger tilting instability for $CsPbBr_3$ (t = 0.86) compared to $CsSnBr_3$ (t = 0.92). This suggests that the stronger tendency for lone-pair driven distortions for Sn^{2+} contributes to the tilting motion, in concert with intra-octahedral distortions at higher frequencies (green lines in Fig. 3(c) and (d)).

We note that there is additional evidence that supports our suggestion that $CsSnBr_3$ exhibits an instability even at 80 K in the orthorhombic phase. Fig. S4 in the ESI† presents the temperature evolution of the Raman spectrum in the 10 K–80 K range. Around 60 K, we find indication of another phase transition to lower symmetry (possibly monoclinic[23]) phase. This phase transition is manifested by the appearance of several new peaks and some changes in the existing modes. Furthermore, Fig. S5 in the ESI† presents 0 K, DFT-based phonon dispersion relations that show imaginary modes for orthorhombic $CsSnBr_3$ but not for orthorhombic $CsPbBr_3$.

Conclusions

Our work illustrates the critical role of the metal cation s lone pairs on the nature of the structural dynamics and represents a first step towards tuning the dynamics of perovskite structures. We investigated how the structural dynamics of $CsMBr_3$ (M = Pb, Sn, and Ge) are affected by the stereochemical electron lone pairs on the metal cations. By simultaneously decreasing the energy scale of the tilting instability and increasing the energy scale of the lone-pair polar distortion across the series $CsPbBr_3$ → $CsSnBr_3$ → $CsGeBr_3$, our primary finding is that for all three compounds, the lone-pair stereochemical activity contributes significantly to octahedral tilting instabilities that are unaccounted for in the geometric models or DFT computations at 0 K. This strong instability leads to liquid-like (*i.e.* central peak) Raman activity in the cubic phase of all three crystals. Since the octahedral tilt angles directly control carrier transport, this study provides the crucial link between chemical composition and optoelectronic properties, opening opportunities for lead-free solution-processable photovoltaics.

Conflicts of interest

There are no conflicts of interest to declare.

Acknowledgements

O. Y. acknowledges funding from BSF (grant No. 2016650) and ERC (850041–ANHARMONIC). D. H. F. gratefully acknowledges financial support from the Alexander von Humboldt Foundation. M. G. K. acknowledges support form the Department of Energy, Office of Science, Basic Energy Sciences, under Grant No. SC0012541 (sample synthesis, structure and property characterization). L. G. was supported by the U.S. Department of Energy, Office of Science, Basic Energy Sciences, under Award # DE-FG02-07ER46431. Computational support was provided by the National Energy Research Scientific Computing Center (NERSC), a U.S. Department of Energy, Office of Science User Facility located at Lawrence Berkeley National Laboratory, operated under Contract No. DE-AC02-05CH11231. A.M.R. acknowledges the support of the Office of Naval Research, under grant number N00014-20-1-2701.

References

1 M. Grätzel, *Acc. Chem. Res.*, 2017, **50**, 487.
2 M. A. Green, E. D. Dunlop, J. Hohl-Ebinger, M. Yoshita, N. Kopidakis and X. Hao, *Prog. Photovoltaics*, 2020, **28**, 629.
3 J. Liang, P. Zhao, C. Wang, Y. Wang, Y. Hu, G. Zhu, L. Ma, J. Liu and Z. Jin, *J. Am. Chem. Soc.*, 2017, **139**, 14009.
4 F. Liu, C. Ding, Y. Zhang, T. S. Ripolles, T. Kamisaka, T. Toyoda, S. Hayase, T. Minemoto, K. Yoshino and S. Dai, *et al.*, *J. Am. Chem. Soc.*, 2017, **139**, 16708.
5 F. Yang, D. Hirotani, G. Kapil, M. A. Kamarudin, C. H. Ng, Y. Zhang, Q. Shen and S. Hayase, *Angew. Chem.*, 2018, **130**, 12927.
6 T. Krishnamoorthy, H. Ding, C. Yan, W. L. Leong, T. Baikie, Z. Zhang, M. Sherburne, S. Li, M. Asta and N. Mathews, *et al.*, *J. Mater. Chem. A*, 2015, **3**, 23829.
7 I. Kopacic, B. Friesenbichler, S. F. Hoefler, B. Kunert, H. Plank, T. Rath and G. Trimmel, *ACS Appl. Energy Mater.*, 2018, **1**, 343.
8 R. Sharma, Z. Dai, L. Gao, T. M. Brenner, L. Yadgarov, J. Zhang, Y. Rakita, R. Korobko, A. M. Rappe and O. Yaffe, *Phys. Rev. Mater.*, 2020, **4**, 092401.
9 O. Yaffe, Y. Guo, L. Z. Tan, D. A. Egger, T. Hull, C. C. Stoumpos, F. Zheng, T. F. Heinz, L. Kronik, M. G. Kanatzidis, J. S. Owen, A. M. Rappe, M. A. Pimenta and L. E. Brus, *Phys. Rev. Lett.*, 2017, **118**, 136001.
10 M. Z. Mayers, L. Z. Tan, D. A. Egger, A. M. Rappe and D. R. Reichman, *Nano Lett.*, 2018, **18**, 8041.
11 A. Lacroix, G. T. de Laissardière, P. Quémerais, J.-P. Julien and D. Mayou, *Phys. Rev. Lett.*, 2020, **124**, 196601.
12 A. Poglitsch and D. Weber, *J. Chem. Phys.*, 1987, **87**, 6373.
13 P. Whitfield, N. Herron, W. Guise, K. Page, Y. Cheng, I. Milas and M. Crawford, *Sci. Rep.*, 2016, **6**(35685), 1.
14 M. Keshavarz, M. Ottesen, S. Wiedmann, M. Wharmby, R. Küchler, H. Yuan, E. Debroye, J. A. Steele, J. Martens, N. E. Hussey, M. Bremholm, M. B. J. Roeffaers and J. Hofkens, *Adv. Mater.*, 2019, **31**, 1900521.
15 S. Maheshwari, M. B. Fridriksson, S. Seal, J. Meyer and F. C. Grozema, *J. Phys. Chem. C*, 2019, **123**, 14652.
16 A. C. Ferreira, S. Paofai, A. Létoublon, J. Ollivier, S. Raymond, B. Hehlen, B. Rufflé, S. Cordier, C. Katan, J. Even and P. Bourges, *Commun. Phys.*, 2020, **3**, 48.
17 W. Chu, Q. Zheng, O. V. Prezhdo, J. Zhao and W. A. Saidi, *Sci. Adv.*, 2020, **6**, eaaw7453.
18 B. Saparov and D. B. Mitzi, *Chem. Rev.*, 2016, **116**, 4558.
19 V. M. Goldschmidt, *Naturwissenschaften*, 1926, **21**, 477.
20 L. Pauling, *J. Am. Chem. Soc.*, 1929, **51**, 1010.
21 A. M. Glazer, *Acta Crystallogr.*, 1972, **28**, 3384.
22 P. M. Woodward, *Acta Crystallogr., Sect. B: Struct. Sci.*, 1997, **53**, 32.
23 C. J. Howard and H. T. Stokes, *Acta Crystallogr., Sect. B: Struct. Sci.*, 1998, **54**, 782.
24 J. Klarbring and S. I. Simak, *Phys. Rev. B*, 2018, **97**, 024108.
25 G. J. Ackland and M. C. Warren, *Phase Transitions*, 1997, **61**, 215.
26 J.-J. Zhou, O. Hellman and M. Bernardi, *Phys. Rev. Lett.*, 2018, **121**, 226603.
27 W. Zhong, D. Vanderbilt and K. M. Rabe, *Phys. Rev. Lett.*, 1994, **73**, 1861.
28 A. Kania, K. Roleder, G. E. Kugel and M. D. Fontana, *J. Phys. C: Solid State Phys.*, 1986, **19**, 9.
29 J. P. Sokoloff, L. L. Chase and L. A. Boatner, *Phys. Rev. B: Condens. Matter Mater. Phys.*, 1990, **41**, 2398.
30 J.-H. Ko, S. Kojima, T.-Y. Koo, J. H. Jung, C. J. Won and N. J. Hur, *Appl. Phys. Lett.*, 2008, **93**, 102905.
31 V. K. Malinovsky, A. M. Pugachev, V. A. Popova, N. V. Surovtsev and S. Kojima, *Ferroelectrics*, 2013, **443**, 124.
32 R. X. Yang, J. M. Skelton, E. L. Da Silva, J. M. Frost and A. Walsh, *J. Phys. Chem. Lett.*, 2017, **8**, 4720.
33 A. N. Beecher, O. E. Semonin, J. M. Skelton, J. M. Frost, M. W. Terban, H. Zhai, A. Alatas, J. S. Owen, A. Walsh and S. J. Billinge, *ACS Energy Lett.*, 2016, **1**, 880.
34 T. Baikie, Y. Fang, J. M. Kadro, M. Schreyer, F. Wei, S. G. Mhaisalkar, M. Grätzel and T. J. White, *J. Mater. Chem. A*, 2013, **1**, 5628.
35 M. C. Alvarez-Galván, J. A. Alonso, C. A. López, E. López-Linares, C. Contreras, M. J. Lázaro, F. Fauth and M. V. Martínez-Huerta, *Cryst. Growth Des.*, 2019, **19**, 918.
36 J. Klarbring, O. Hellman, I. A. Abrikosov and S. I. Simak, *Phys. Rev. Lett.*, 2020, **125**, 045701.
37 J. A. Brehm, J. W. Bennett, M. R. Schoenberg, I. Grinberg and A. M. Rappe, *J. Chem. Phys.*, 2014, **140**, 224703.
38 C. Li, K. C. K. Soh and P. Wu, *J. Alloys Compd.*, 2004, **372**, 40.
39 L. Feng, L. Jiang, M. Zhu, H. Liu, X. Zhou and C. Li, *J. Phys. Chem. Solids*, 2008, **69**, 967.
40 C. Li, X. Lu, W. Ding, L. Feng, Y. Gao and Z. Guo, *Acta Crystallogr., Sect. B: Struct. Sci.*, 2008, **64**, 702.
41 W. Travis, E. Glover, H. Bronstein, D. Scanlon and R. Palgrave, *Chem. Sci.*, 2016, **7**, 4548.

42 M. R. Filip and F. Giustino, *Proc. Natl. Acad. Sci. U. S. A.*, 2018, **115**, 5397.
43 F. R. Poulsen and S. E. Rasmussen, *Acta Chem. Scand.*, 1970, **24**, 150.
44 P. Berastegui, S. Hull and S.-G. Eriksson, *J. Phys.: Condens. Matter*, 2001, **13**, 5077.
45 I. Grinberg and A. M. Rappe, *Phase Transitions*, 2007, **80**, 351.
46 G. Laurita, D. H. Fabini, C. C. Stoumpos, M. G. Kanatzidis and R. Seshadri, *Chem. Sci.*, 2017, **8**, 5628.
47 M. G. Goesten and R. Hoffmann, *J. Am. Chem. Soc.*, 2018, **140**, 12996.
48 D. H. Fabini, R. Seshadri and M. G. Kanatzidis, *MRS Bull.*, 2020, **45**, 467.
49 J. Galy, G. Meunier, S. Andersson and A. Åström, *J. Solid State Chem.*, 1975, **13**, 142.
50 U. V. Waghmare, N. A. Spaldin, H. C. Kandpal and R. Seshadri, *Phys. Rev. B: Condens. Matter Mater. Phys.*, 2003, **67**, 125111.
51 A. Walsh and G. W. Watson, *J. Phys. Chem. B*, 2005, **109**, 18868.
52 A. Walsh, D. J. Payne, R. G. Egdell and G. W. Watson, *Chem. Soc. Rev.*, 2011, **40**, 4455.
53 M. W. Stoltzfus, P. M. Woodward, R. Seshadri, J.-H. Klepeis and B. Bursten, *Inorg. Chem.*, 2007, **46**, 3839.
54 S.-E. Park and T. R. Shrout, *J. Appl. Phys.*, 1997, **82**, 1804.
55 R. Seshadri, *Proc. - Indian Acad. Sci., Chem. Sci.*, 2001, **113**, 487.
56 B. Noheda, *Curr. Opin. Solid State Mater. Sci.*, 2002, **6**, 27.
57 I. Grinberg, V. R. Cooper and A. M. Rappe, *Nature*, 2002, **419**, 909.
58 Y. Uratani, T. Shishidou and T. Oguchi, *Jpn. J. Appl. Phys.*, 2008, **47**, 7735.
59 W. M. A. Smit, G. J. Dirksen and D. J. Stufkens, *J. Phys. Chem. Solids*, 1990, **51**, 189.
60 H. Ishida, H. Maeda, A. Hirano, Y. Kubozono and Y. Furukawa, *Phys. Status Solidi A*, 1997, **159**, 277.
61 R. J. Worhatch, H. Kim, I. P. Swainson, A. L. Yonkeu and S. J. Billinge, *Chem. Mater.*, 2008, **20**, 1272.
62 S. Liu, F. Zheng, N. Z. Koocher, H. Takenaka, F. Wang and A. M. Rappe, *J. Phys. Chem. Lett.*, 2015, **6**, 693, DOI: 10.1021/jz502666j.
63 D. H. Fabini, G. Laurita, J. S. Bechtel, C. C. Stoumpos, H. A. Evans, A. G. Kontos, Y. S. Raptis, P. Falaras, A. Van der Ven, M. G. Kanatzidis and R. Seshadri, *J. Am. Chem. Soc.*, 2016, **138**, 11820.
64 J. Liu, A. E. Phillips, D. A. Keen and M. T. Dove, *J. Phys. Chem. C*, 2019, **123**, 14934.
65 R. C. Remsing and M. L. Klein, *Phys. Rev. Lett.*, 2020, **124**, 066001.
66 R. C. Remsing and M. L. Klein, *APL Mater.*, 2020, **8**, 50902.
67 E. H. Smith, N. A. Benedek and C. J. Fennie, *Inorg. Chem.*, 2015, **54**, 8536.
68 S. K. Radha, C. Bhandari and W. R. Lambrecht, *Phys. Rev. Mater.*, 2018, **2**, 063605.
69 I. Grinberg, M. R. Suchomel, P. K. Davies and A. M. Rappe, *J. Appl. Phys.*, 2005, **98**, 094111.
70 R. X. Yang, J. M. Skelton, E. L. Da Silva, J. M. Frost and A. Walsh, *J. Chem. Phys.*, 2020, **152**, 024703.
71 A. Maalej, Y. Abid, A. Kallel, A. Daoud, A. Lautié and F. Romain, *Solid State Commun.*, 1997, **103**, 279.
72 K. Nakamoto, Applications in inorganic chemistry, *Infrared and Raman Spectra of Inorganic and Coordination Compounds*, John Wiley & Sons, Ltd, 2008, ch. 2, pp. 149–354.
73 C. C. Stoumpos, L. Frazer, D. J. Clark, Y. S. Kim, S. H. Rhim, A. J. Freeman, J. B. Ketterson, J. I. Jang and M. G. Kanatzidis, *J. Am. Chem. Soc.*, 2015, **137**, 6804.
74 G. Thiele, H. W. Rotter and K. D. Schmidt, *Z. Anorg. Allg. Chem.*, 1987, **545**, 148.
75 T. Lanigan-Atkins, X. He, M. J. Krogstad, D. M. Pajerowski, D. L. Abernathy, G. N. M. N. Xu, Z. Xu, D.-Y. Chung, M. G. Kanatzidis, S. Rosenkranz, R. Osborn and O. Delaire, *Nat. Mater.*, 2021, DOI: 10.1038/s41563-021-00947-y.
76 X. Lü, C. Stoumpos, Q. Hu, X. Ma, D. Zhang, S. Guo, J. Hoffman, K. Bu, X. Guo, Y. Wang, C. Ji, H. Chen, H. Xu, Q. Jia, W. Yang, M. G Kanatzidis and H.-K. Mao, *Natl. Sci. Rev.*, 2021, nwaa288.